Biophysical Journal Volume 107 October 2014 1980–1987

Article

Direct Measurements of Drag Forces in *C. elegans* Crawling Locomotion

Yegor Rabets,[1,2] Matilda Backholm,[3] Kari Dalnoki-Veress,[3,4] and William S. Ryu[1,2,5,*]

[1]Institute of Biomaterials and Biomedical Engineering and [2]Donnelly Centre for Cellular and Biomolecular Research, University of Toronto, Toronto, Ontario, Canada; [3]Department of Physics & Astronomy and the Brockhouse Institute for Materials Research, McMaster University, Hamilton, Ontario, Canada; [4]Laboratoire de Physico-Chimie Théorique, UMR Centre National de la Recherche Scientifique 7083 GULLIVER, ESPCI, Paris, France; and [5]Department of Physics, University of Toronto, Toronto, Ontario, Canada

ABSTRACT With a simple and versatile microcantilever-based force measurement technique, we have probed the drag forces involved in *Caenorhabditis elegans* locomotion. As a worm crawls on an agar surface, we found that substrate viscoelasticity introduces nonlinearities in the force-velocity relationships, yielding nonconstant drag coefficients that are not captured by original resistive force theory. A major contributing factor to these nonlinearities is the formation of a shallow groove on the agar surface. We measured both the adhesion forces that cause the worm's body to settle into the agar and the resulting dynamics of groove formation. Furthermore, we quantified the locomotive forces produced by *C. elegans* undulatory motions on a wet viscoelastic agar surface. We show that an extension of resistive force theory is able to use the dynamics of a nematode's body shape along with the measured drag coefficients to predict the forces generated by a crawling nematode.

INTRODUCTION

We present here an experiment to directly measure forces on the body of *Caenorhabditis elegans* as it moves on a surface of a hydrogel. This model organism is a small (~1 mm) nematode that moves by propagating quasi-sinusoidal bending waves along its body. This oscillatory movement pattern is a general locomotory strategy employed by an enormous variety of animals spanning a wide range of size scales and habitats, from spermatozoa (1) and fish (2) in aqueous environments to snakes (3) and sandfish lizards (4) on solid and granular terrestrial systems. Nematodes have evolved to move in a variety of complex environments from fresh compost (5) and rotting fruit (6) to wet soils (7), plant stalks (8), and the exoskeletons of gastropods (6). In the lab, *C. elegans* is studied primarily on the surface of agar plates, where it moves in a thin water layer that forms on top of the moisture-saturated viscoelastic polysaccharide gel. Although this is seemingly a simple environment, the thinness of the liquid layer and the deformability of agar both contribute to the complex mechanics of this system. Many theoretical treatments of *C. elegans* motions have been attempted (9–12), but few direct measurements of the forces involved have been made (13,14).

Through the pioneering work of Gray (3), we know that the directed thrust from undulations of a slender organism comes from the differential resistive forces on the organism's body as it performs its wavelike motions. Here we are not concerned with the physiological mechanism (muscles, neurons, etc.) generating the undulatory motions, but with how these motions interact with the external environment to provide a net propulsive force. For large organisms moving in rigid environments, the theoretical and experimental study of locomotion mechanics is relatively straightforward; however, when the organism is small and is interacting with fluid, a number of assumptions are necessary to make the problem tractable. In the simplest treatment, Gray and Hancock (1) used resistive force theory (RFT) to analyze each segment of a long and slender body independently. Specifically, when worms crawl ($u \sim 300$ μm/s) in a thin ($h \sim 10$ μm), viscous ($\nu \sim 10^{-6}$ m^2/s) fluid layer, the motion is at low Reynolds number ($Re \sim 0.01$).

On the microscale, RFT makes use of the low Re approximation by linearly relating the forces exerted on the surrounding viscous fluid to the normal and tangential velocities v_n and v_t relative to the fluid, such that $F_t = \mu C_t v_t L$ and $F_n = \mu C_n v_n L$. Here, μ is the dynamic viscosity, C_t and C_n are the drag coefficients, and F_t and F_n are the forces exerted by a body segment tangentially and normally to an organism's body. RFT had initially been developed for swimmers in perfectly viscous media and for macroscopic terrestrial crawlers on solid surfaces (1,15,16), but more recently it had been extended to slender macroscopic undulators on granular media (4,17), flat surfaces (18) and in muds (19). Whereas original formulations of RFT in wet media were for bodies immersed in infinite homogeneous liquids, the same ideas could presumably be adapted to lubricated crawling environments.

One of the challenges in developing a theoretical framework for undulatory locomotion on non-Newtonian surfaces and in thin films has been the difficulty in obtaining drag coefficients. Several studies have attempted to

Submitted June 19, 2014, and accepted for publication September 3, 2014.

*Correspondence: wryu@physics.utoronto.ca

Editor: Charles Wolgemuth.

0006-3495/14/10/1980/8 $2.00

http://dx.doi.org/10.1016/j.bpj.2014.09.006

calculate drag coefficients with a theoretical approach. Shen et al. (10) considered the viscoelastic substrate as a static surface by imposing a constant groove shape in their calculations, and obtained a linear force-velocity relationship (as in RFT). Sauvage et al. (11) did not consider gel indentation and were thus unable to predict drag coefficient ratios >2, which should be possible in non-Newtonian media. Wallace (20) obtained the first empirical estimates of drag forces for microcrawlers by displacing nematode-sized glass rods, which were initially at rest, across agar surfaces. However, the force required to dislodge a stationary object on agar is likely not the same as the force required to keep the object in motion, and the surface properties of the probe likely differ from those of *C. elegans*' body. Much of the other literature (21–23) dealing with crawling locomotion makes use of the approximation of Gray and Lissmann (24) of the drag coefficient ratio based on slip percentage.

In this article, we utilize a simple technique for measuring drag forces involved in the locomotion of microorganisms. With calibrated micropipette cantilevers, we directly measure drag on nematodes as they slide on wet surfaces. Instead of a proxy of the nematode body, we use the organism itself to ensure the consistency of wettability and other surface interactions that are likely important at this scale. These measurements enable the biomechanical analysis of *C. elegans* locomotion on this common laboratory medium. We also measure and discuss several physical factors contributing to locomotory drag forces. Finally, using these results we implement a generalized variant of RFT to calculate the force generated by an undulating microcrawler simply from observations of body shape.

METHODS

Tool and sample preparation

Force-sensing pipettes were manufactured from borosilicate capillaries and calibrated according to a protocol developed by Colbert et al. (25). Tip widths of the cantilever pipettes were ~30–50 μm for drag speeds >500 μm/s, and 20–40 μm for lower speeds. With cantilever lengths of 15–20 mm, the measured spring constants were between 60 and 350 nN/μm with an uncertainty of <3%. For crawl force measurements, pipettes were calibrated for stiffness both parallel (k_{par} ~ 300–550 nN/μm) and perpendicular (k_{perp} ~ 150–220 nN/μm) to the long capillary axis (see Fig. 1 *A* for a rendering of pipette setup).

Nematode growth medium (NGM) with varying agar concentrations (BP1423; Fisher Scientific, Fair Lawn, NJ) but without buffers was prepared all at once and stored in aliquots. Each aliquot was reheated, had 5 mg/L cholesterol and buffers (25 mM KPO_4, 1 mM $CaCl_2$, 1 mM $MgSO_4$) added when cooled to 55°C, and was poured daily into 5 mL plates 3 h before assaying. Plates were then allowed to dry for 15 min before commencing experiments, which were conducted at room temperature (23 ± 1.5°C) and were limited to 30 min to keep the loss of water mass <5%.

Young adult N2 wild-type worms, acquired from the Caenorhabditis Genetics Center, were cultivated according to standard methods (26) on *Escherichia coli* (OP50) NGM plates at 20°C.

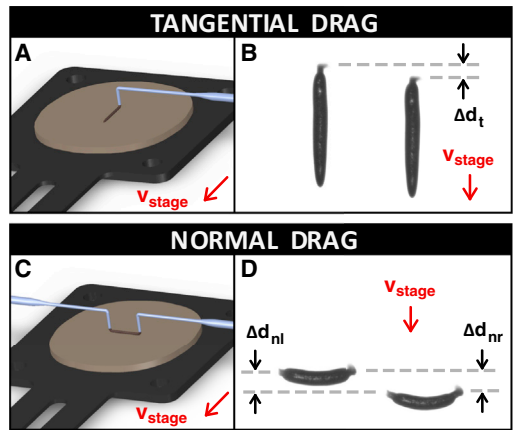

FIGURE 1 Experimental setup for direct drag force measurements. (*A* and *C*) Suction applied through cantilevered micropipettes is used to hold worms by the tail or by both head and tail for tangential and normal drag, respectively. The v_{stage} points in the direction of stage movement. (*B* and *D*) Raw video data of the worm before and after initiating stage translation at a fixed velocity. Displacement Δd_t of the pipette tip in panel *B* and the pipette's stiffness constant Δk_t are used to calculate instantaneous forces during tangential drag. For normal drag in panel *D*, the resulting force is calculated from tip displacements Δd_{nl} and Δd_{nr} and stiffness constants k_{nl} and k_{nr}, corresponding to left and right pipettes, respectively.

Drag measurements

Worms on NGM plates were transiently paralyzed via immersion in a 0.5 μL drop of 3 mM Levamisole hydrochloride (31742; Sigma-Aldrich, St. Louis, MO). Once the drop absorbed into the agar, animals were captured and held with light suction by calibrated pipettes filled with M9 buffer (see Fig. 1, *A* and *C*). Each worm was predragged on clean NGM for at least 30 mm (~30 body lengths) to wash off residual Levamisole and to fully elongate the worm before data collection. The plate-holding stage was then translated at fixed speeds by a custom LABVIEW (National Instruments, Austin, TX) script while the cantilevers were held stationary (see Movie S1 and Movie S2 in the Supporting Material). Worms were held by the tail for tangential drag, and by both head and tail for normal drag experiments. All worms recovered from paralysis and were motile within 24 h.

The tangential force is calculated from the pipette's spring constant k_t, its deflection Δd_t (Fig. 1 *B*), and the length of the worm in contact with the agar surface, $L_{contact}$ (in units of micrometers). The force is then extrapolated to a 1-mm worm:

$$F_t = k_t \Delta d_t \left(\frac{1000}{L_{contact}} \right). \quad (1)$$

When dragged normally to their body axis, worms bend in the direction of stage motion (Fig. 1 *D*) and we must factor out any contributing tangential drag components. With θ_t being the angle between the worm's tangent and the predrag worm axis and l the worm's visible body coordinate in micrometers, vector decomposition along the worm body yields

$$F_n = \left(k_{nl} \Delta d_{nl} + k_{nr} \Delta d_{nr} - \frac{F_t(v_{drag})}{1000} \int_0^{L_{contact}} \sin|\theta_t(s)| dl \right) \times \left(\frac{1000}{L_{contact}} \right). \quad (2)$$

Here, k_{nl} and k_{nr} are the left and right pipette stiffnesses, Δd_{nl} and Δd_{nr} are the pipette displacements, and $F_t(v_{drag})$ is the velocity-dependent tangential drag force measurement.

Worm settling measurements

After paralyzing worms, $10 \times 4\,mm^2$ sections of agar were cut out of the plate and placed on a microscope slide for horizontal imaging. Worms were held by a micropipette and dragged into the field of view. The silhouette was imaged for 1 min at 30 frames per second (FPS), and the lowering of the top of the cuticle was assumed to be indicative of increasing groove depth. According to estimates of elastic moduli of ~10 MPa for worms in the circumferential direction (27) and storage and loss moduli of $\sim E' = 400$ kPa and $E'' = 8$ kPa for 1.7% agar (28), it is reasonable to assume that during groove formation the worm is deformed negligibly compared to agar.

The vertical compression of agar due to dehydration was also noted and subtracted from the settling time series. The settling curves were fitted with the Burger model $h_{sink}(t) = h_1(1 + E_1t/\eta_1) + h_2[1 - \exp(-E_2t/\eta_2)]$ shown later in Fig. 3 *D*, where h_{sink} is the settling depth, $\eta_{1,2}$ are viscosities of dashpot elements, $E_{1,2}$ values are the elastic moduli of springs, and h_1 and h_2 are constants. This is the minimal model to capture the observed creep and exponential strain rate decay. Ratios of $\eta_{1,2}/E_{1,2}$ were treated jointly as $\tau_{1,2}$, yielding values of $h_1 = \{-0.82, -0.45, -0.12, -0.14\}$; $h_2 = \{-5.4, -3.9, -2.2, -1.8\}$; $\tau_1 = \{13, 10, 19, 1900\}$; and $\tau_2 = \{1.7, 3.5, 160, 258\}$ for agar concentrations of {1.0, 1.7, 4.0, 6.0%}.

Adhesion force measurements

After paralyzing worms, $10 \times 4\ mm^2$ sections of agar were cut out of the plate and placed on a microscope slide for horizontal imaging. Worms were again held by a calibrated micropipette and slowly lifted off the agar until only the tip of the head (foremost 40 μm) was in contact with the water layer. As the worm pulls off from the surface, the adhesion force can be obtained from the pipette tip displacement. Each worm was only assayed once due to dehydration effects after each trial, and trials were completed within 5 min of cutting out the agar mound.

To extrapolate the adhesion force that acts on the worm's head tip to the force experienced by an entire crawling worm, we must take into account the effects of geometry in each case. Assuming perfect wetting, the azimuthal and meridional radii of the axisymmetric meniscus in our experimental condition can be estimated by $R_{azimuthal} = R_w/\sin\varphi$ and $R_{meridional} = R_w(1 - \cos\varphi)/\sin\varphi(1 + \cos\varphi)$, as prescribed by Orr et al. (29). Here, R_w is the radius of the wetting perimeter on the worm's head and ψ is the fill angle of the head tip, which is approximated as a sphere. The adhesion force on a vertically held worm's head, where σ is the surface tension, is then given by

$$F_{adh,head} = \frac{2\pi\sigma R_w \sin\psi}{1 - \cos\psi}. \quad (3)$$

For a worm positioned horizontally on agar, the force due to surface tension is simply $F_{st} = 2L\sigma\sin\theta_f$ and the capillary force is $F_{cap} = 2\sigma LR\sin\theta_f/r$, where R is the worm radius, r is the radius of curvature of the meniscus, and θ_f is the fill angle on a worm's cross-section (see later in Fig. 4 *B*). Thus,

$$F_{adh,worm} = 2L\sigma\sin\theta_f\left(1 + \frac{R}{r}\right). \quad (4)$$

We then extrapolate our measurement to the force experienced by an entire worm:

$$F_{adh,extrap} = \frac{L\sin\theta_f\left(1 + \frac{R}{r}\right)(1 - \cos\psi)}{\pi R_w \sin\psi} F_{adh,measured}. \quad (5)$$

The fill angle can be found using the groove depth h_{sink}, the thickness h_{liq} of the liquid layer on the agar surface, the meniscus radius r, and the thickness h_0 of the lubrication layer under the center of the worm (see diagram later in Fig. 4 *B*):

$$\theta_f = \cos^{-1}\left(\frac{R + h_0 - h_{liq} - h_{sink} - r}{R + r}\right). \quad (6)$$

We assumed that $r = 5h_{liq}/4$, based on observations. Values for h_{liq} were obtained by lowering the polished flat face of a copper wire rod hung on a micropipette onto the surface of the liquid layer, and noting the sudden displacement upon wetting. Wire diameter was chosen to provide enough surface tension force to pull the probe all the way down to the solid phase of agar.

Imaging of flow patterns around crawling worms

Worms were imaged while crawling on agar plates seeded with a 1:1000 dilution of 1-μm fluorescent polystyrene beads (Bangs Laboratories, Fishers, IN). To analyze trajectories, the speed and distance from the cuticle of single particles were tracked for 1–5 s.

Calculation of crawl forces from body shape measurements

Unanesthetized worms on NGM plates were captured by the tail and held with constant light suction by calibrated pipettes filled with M9 buffer (see Movie S3). Force recordings were started immediately after worms were dragged onto a new region of agar. The worm midline was found with an in-house developed skeletonization algorithm and a cubic spline fit was used to obtain 101 evenly-spaced body segments i. The tangential and normal speeds v_t and v_n of each body segment i at time t were calculated using the segment velocities $\mathbf{v}(i,t)$ and the angle θ_{vt} of segment progression with respect to the worm midline tangent:

$$v_t(i,t) = |\mathbf{v}(i,t)|\cos(\theta_{vt}), v_n(i,t) = |\mathbf{v}(i,t)|\sin(\theta_{vt}). \quad (7)$$

Angle θ_{vt} was found using segment positions $\mathbf{r}(i,t)$:

$$\theta_{vt}(i,t) = \tan^{-1}\{\mathbf{r}(i,t+\delta t) - \mathbf{r}(i,t)\} - \tan^{-1}\{\mathbf{r}(i+1,t) - \mathbf{r}(i,t)\}. \quad (8)$$

Speeds extracted from the midline were smoothed with a Gaussian filter with $\sigma_t = 0.2$ s and $\sigma_x = 4\%$ of body length to reduce imaging and skeletonization noise. The drag force-to-velocity mappings αv^γ were taken from empirical fits for α and γ of the drag force measurement data for agar concentrations of {1.0, 1.7, 3.0, 4.0, 6.0%}; $\alpha_t = \{0.35, 0.32, 0.26, 0.24, 0.20\}$; $\alpha_n = \{4.6, 6.8, 7.9, 7.3, 5.8\}$; $\gamma_t = \{0.55, 0.58, 0.68, 0.77, 0.81\}$; and $\gamma_n = \{0.27, 0.31, 0.30, 0.34, 0.38\}$. Thus, for each body segment at a given time t, with θ_t being the worm midline tangent,

$$F_{x,recon} = \sum_{i=0}^{100}\{\alpha_t v_t(i)^{\gamma_t}\sin[\theta_t(i)] + \alpha_n v_n(i)^{\gamma_n}\cos[\theta_t(i)]\}, \quad (9)$$

$$F_{z,recon} = \sum_{i=0}^{100}\{\alpha_t v_t(i)^{\gamma_t}\cos[\theta_t(i)] - \alpha_n v_n(i)^{\gamma_n}\sin[\theta_t(i)]\}. \quad (10)$$

The reconstruction was shifted by an additional phase parameter to account for the phase offset between undulatory motion and the generated force.

This phase lag develops for any system in a resistive force medium, and depends on both the medium properties and locomotion parameters (30).

Image acquisition and processing

Forces in the main drag experiment, the adhesion force, and the crawl force experiments were recorded with the software LABVIEW (National Instruments) and a custom imaging system consisting of a 90-mm focal length imaging lens (MMS; Edmund Optics, Barrington, NJ) mounted on a Manta G-125 charge-coupled device camera (Allied Vision Technologies, Stadtroda, Germany). Worm settling images, meniscus images for the adhesion force, and flow pattern images were taken with a model No. M205 FA stereo microscope (Leica, Solms, Germany) at 256× magnification (75× for flow patterns). Drag images captured at 30 FPS were processed with custom MATLAB (The MathWorks, Natick, MA) scripts to extract the pipette deflection for each trial.

RESULTS

Drag coefficients are velocity-dependent on viscoelastic surfaces

In laboratory conditions on standard agar plates, young adult *C. elegans* typically travel at 80–300 μm/s, depending on numerous factors such as the immediate presence of food (31), temperature fluctuations (32), starvation state (31), or dopamine balance (33). *C. elegans* can move up to 0.8 mm/s during its escape response (34), so we assayed drag forces at speeds up to 1 mm/s. As expected for organisms that generate thrust opposite to the direction of propagated undulations (1), the normal drag for each condition is higher than the tangential drag (Fig. 2). Additionally, drag forces increase on gels with higher agar concentration and do not scale linearly with velocity. This nonlinearity implies that drag coefficients C_n and C_t are not constant, and this is especially prevalent in the regime of typical *C. elegans* locomotion speeds. Inasmuch as the normal and tangential speeds of worm segments constantly fluctuate out of phase, a global drag coefficient ratio C_n/C_t cannot be defined (Fig. 2, *inset*).

Interestingly, for each condition the ratios of slopes for the high-speed portions (>500 μm/s) of the normal versus tangential drag curves are 1.4 ± 0.2. Thus, if the force-velocity curves are extrapolated to infinity, the drag coefficient ratios would asymptotically approach ~1.4. This is close to the value of 1.5 initially suggested by Gray and Lissmann (24) and confirmed with both extrapolations from kinematic data (13) and direct measurements (14) for swimming nematodes. In contrast to the convergence toward swimmerlike slope ratios at high drag speeds, the deviation of drag curves from linearity at low speeds suggests the worm encounters the non-Newtonian material properties predominantly in the low-speed regime.

Dynamics of groove formation

The increase of drag coefficients on agar has been widely attributed to the carving of grooves by crawling worms. Our drag experiment provides a visual confirmation of groove formation: notably, traces left behind by stationary animals are significantly wider than those left behind by moving animals (Fig. 3 *A*). From our measurements of worm settling (Fig. 3 *B*), we observed that, in addition to sinking to appreciable depths, worms sink slowly on timescales that are comparable to their locomotive speed. On softer gels, the sinking time constants are $\tau \sim 1$–3 s, which is similar to the time it takes a young adult to move one body length. Because there is little slip at most points along the worm's trajectory, the tail mostly follows the head. The tails of slower-moving worms will sink deeper into the agar, making the groove profile—and consequently the drag coefficients—velocity-dependent.

The dynamics of groove formation are governed by adhesion forces pinning the worm to the surface, the worm's contact geometry, and the substrate viscosity. The adhesion force, comprised of surface tension and capillary pressure components (29), is experimentally found to increase with increasing agar concentration (Fig. 4 *D*). This agrees with

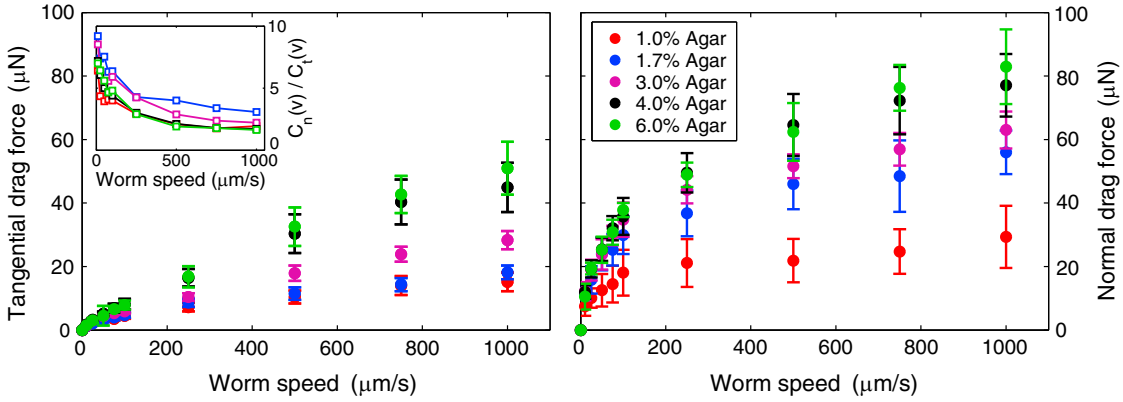

FIGURE 2 Measurements of tangential and normal drag forces as a function of speed on gels with different agar concentrations. Error bars: SD. (*Inset*) Ratios of the normal to tangential drag coefficients as a function of drag speed.

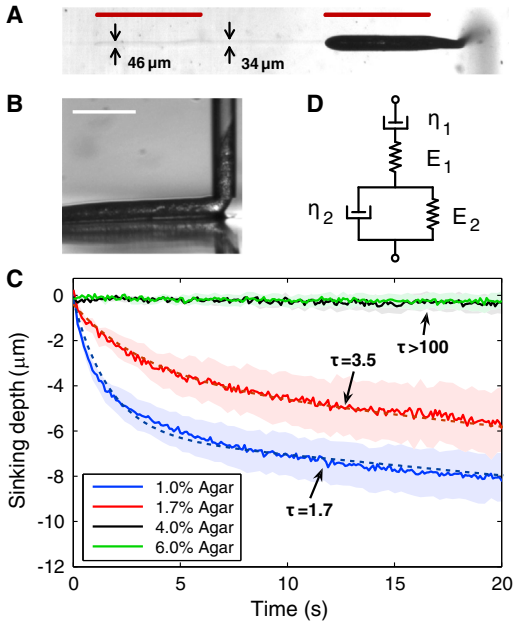

FIGURE 3 Characterizing the settling of worms into viscoelastic substrates. (*A*) Worms leave wider grooves after resting on the surface longer. The left portion of the trace was left behind by a worm left at rest on an agar surface for >1 min. The middle (34-μm wide) portion of the trace was left within several seconds of capturing the image by the worm as it is translated to the right. (*B*) Anesthetized worms were dragged into the field of view with a micropipette and imaged horizontally. Scale bar: 200 μm. (*C*) On soft (1.0%) and standard (1.7%) agar gels, worms settle with time constants of several seconds; (*shaded areas*) SD. (*Dashed lines*) Fits using the Burger model and $\tau = \eta_2/E_2$. (*D*) Schematic of the viscoelastic model for fits in panel *C*.

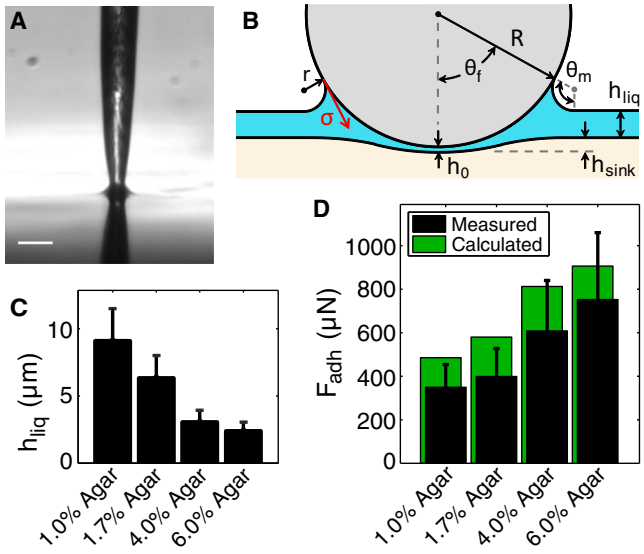

FIGURE 4 Experimental and theoretical estimates of adhesion force acting on crawling nematodes. (*A*) To measure the adhesion force, worms were aligned so that only the tip of the head contacted the liquid layer, and were slowly pulled off the agar while recording force on the lifting pipette. Scale bar: 50 μm. (*B*) Schematic cross section of a nematode sliding on a wet deformable surface. (*C*) Measurements of the depth of the liquid layer forming on an agar gel surface. Error bars: SD. (*D*) Adhesion force measurements and theoretically estimated values from geometry in panels *A* and *B*; error bars represent the uncertainty due to pipette calibration and estimation of angles from images.

the intuition of Wallace (7), who suggested that very thin liquid films pin nematodes to the surface with large force. The trend can be confirmed with simple geometrical arguments using the fill angle θ_f, worm radius R, meniscus radius r, surface tension σ, and worm length L (Eq. 4 and Fig. 4 *B*). The value θ_f further depends on the liquid layer depth h_{liq} (which increases on less concentrated agar gels because of reduced water capacity; see Fig. 4 *C*), R and r (Eq. 5).

How does groove formation affect drag forces?

Based on our observations of groove formation, we expect that at slower speeds the groove profile should approach the circumferential curvature of the worm and thus on average decrease the lubrication film thickness h under the worm. Assuming a simple parallel plate shear analogy used by Shen et al. (10) for tangential drag, the tangential drag force should be proportional to the mean inverse of film thickness. However, the force estimate from this parallel plate model is sensitive to the lubrication layer depth profile h, which we could not measure. To assess how drag forces are affected in different environments without relying on measurements of h, we quantified the nonlinearities in each drag force-velocity curve. The curves are well fitted empirically ($r^2 > 0.95$) by power-law relationships of the form $F = \alpha v^{\gamma}$ (Fig. 5). For analytical convenience, this can be decomposed into a typical RFT-like linear component with slope α' and a modulation envelope in which β is the envelope normalization factor:

$$F_{t,n} = \alpha'_{t,n} v_{t,n} \left(\beta_{t,n} v_{t,n}^{-\left(1-\gamma_{t,n}\right)} \right).$$

The envelope exponent $1-\gamma$ is an index of nonlinearity. Positive indices imply monotonically decreasing envelope functions (as observed), negative indices imply increasing envelopes, and an index of zero produces a purely linear drag curve. The nonlinearity index is small on hard gels, increases on softer gels, and is generally larger for normal than tangential drag. This is consistent with our expectations that groove formation would most affect normal drag on softer surfaces.

Following the parallel plate shear analogy, we would expect that a worm traveling at a given speed on a softer substrate would sink deeper and thus experience higher drag forces than on a stiffer substrate. Our measurements, however, show the opposite; clearly the parallel plate analogy alone is not sufficient. In addition to mechanical properties, changing agar concentration also changes the depth of the liquid layer forming on the agar surface. To examine how this liquid layer affects drag forces, we tracked fluorescent

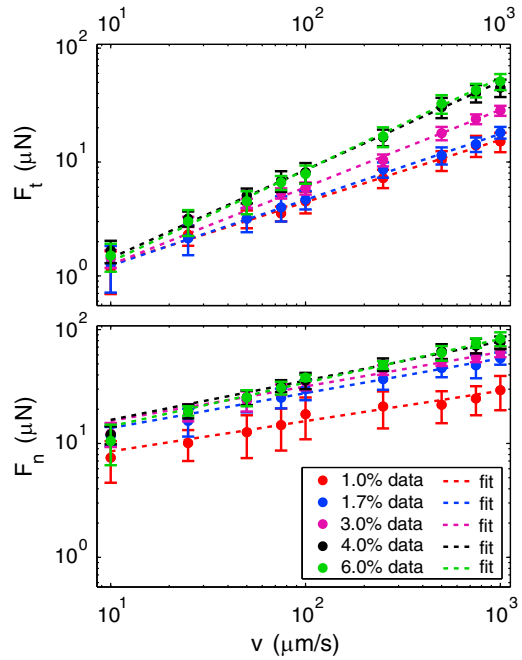

FIGURE 5 Quantifying nonlinearities in drag force curves. $1-\gamma$ (where γ is the scaling exponent) yields the nonlinearity index for each data series. An index of 0 indicates a purely linear relationship; greater absolute values signify larger deviations from linearity (here, data with shallower slopes are less linear). Positive indices mean that curves are sublinear. $1-\gamma_t = \{0.45, 0.42, 0.32, 0.23, 0.19\}$ and $1-\gamma_n = \{0.73, 0.69, 0.70, 0.66, 0.62\}$ for agar concentrations of {1.0, 1.7, 3.0, 4.0, 6.0%}. Note that this is the same data from Fig. 2 but on a log-log scale.

beads around crawling nematodes. In environments where the liquid film is thinner (higher agar concentrations), fluid displacement seems to be limited to a proximal vicinity around the worm. On average, the distance from the cuticle $d_{v_{worm}/2}$ at which particle velocity drops off to half the nematode speed is much higher on deeper fluid films ($d_{v_{worm}/2} \approx$ 44, 24, 11, and 9 μm for 1, 1.7, 4, and 6% agar, respectively). Thus it appears that the dissipation of a nematode's propulsive energy extends beyond the lubrication layer directly below the cuticle. The larger horizontal shear gradients on surfaces with shallower liquid layers will lead to increased forces in these conditions.

Calculation of locomotory forces from the body shape dynamics

According to RFT, in the viscous regime it should be possible to calculate forces produced by slender undulating organisms based on the movements of their body and the measured drag coefficients associated with the medium. More specifically, given the tangential and normal velocities of each body segment and a mapping of velocities to forces in a particular medium, the forces generated by the body can be calculated. The force-velocity mapping is given by the previously described empirical fits of drag force curves, and is of the form $F = \alpha v^{\gamma}$, which adequately captures the velocity dependence of the drag coefficients.

Force was recorded by holding the worm's tail with a calibrated micropipette while the normal and tangential velocities of body segments were simultaneously extracted from image sequences of the worm's crawling movements (Fig. 6 *A*). Because of the imposed physical constraint, worms typically undulated with roughly half the frequency of freely-crawling wild-type worms and with reduced amplitude in the tail region. Sinusoidal oscillations were still properly propagated posteriorly from the head, but inasmuch as worms were prevented from translating by the micropipette cantilever, their motions were punctuated by additional backward slip compared to unrestricted movement. The force reconstruction generally yielded fits within error of the force observed from recordings at the tail (root-mean square of residuals was on average 74% of reconstruction uncertainty for 19 recordings).

Lateral forces F_x were quasi-sinusoidal and nearly centered around the propulsive axis. Propulsive forces F_y generally exhibited smaller amplitude fluctuations centered around a constant offset (Fig. 6 *B*), typically with more force generated during ventral bends. The average exerted force is several times smaller than that observed in a

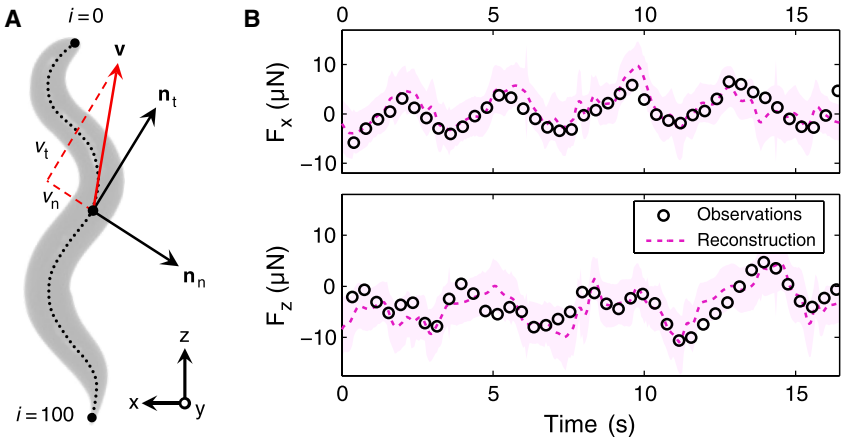

FIGURE 6 Reconstruction of forces exerted by a nematode during crawling. (*A*) Schematic of crawl force measurement and definition of speeds v_n and v_t in the normal ($\mathbf{n}_n$) and tangential ($\mathbf{n}_t$) coordinate axes, respectively. Worms were held by the tail, at $i = 100$. (*B*) Reconstruction of crawling forces from measured force-velocity relationships. (*Shaded region*) Uncertainty arising from the fits for force-velocity mapping parameters, and from calculating angles and velocities from worm images.

microstructured pillar environment (35), but this is expected because the main resistive medium on agar is liquid. Some of the discrepancy between measured and mathematically reconstructed forces arises from the worm's head's foraging movements, because it is sometimes unclear whether the worm's head is elevated off the agar. During unrestricted motion, the tail is not an imposed node; thus, less of the overall force is generated in the anterior region and this source of error is expected to be less significant.

DISCUSSION

With a simple and versatile force measurement technique, we have probed the drag forces involved in *C. elegans* locomotion. The glass microcapillary probes are tunable across a wide range of forces simply by adjusting geometry, and have been used to measure biomechanical properties of nematodes (36), adhesion properties of vesicles, cells and cellular aggregates (25,37,38), and cellular deformation in response to stiffness (39). The drag force measurements, which have been sought since 50 years ago (24), are an important step toward a complete understanding of behavior in a model metazoan.

The formation of grooves during crawling on viscoelastic surfaces has previously been noted (24) and incorporated into models as a static process (10) or a single number (9,11). However, we observed that the settling of nematodes into agar occurs on timescales similar to nematode movement. Thus, we note that to understand the effects of grooves on local drag forces, it is imperative to consider the dynamics of groove formation. The local settling depth will be affected by the amount of time a nematode body contacts the area, and should thus depend on crawling speed and position along the worm body. Furthermore, the settling of the worm into the groove implies that when considering the hydrodynamics of the lubrication layer, forces in the vertical axis do not need to be balanced, as was assumed previously in several theoretical articles (10,11). Because the adhesion forces we measured are an order-of-magnitude higher than the propulsive forces generated by the worm, we suggest that groove formation is due largely to surface tension. Hence, the worm "settles" into a groove and does not carve it.

Producing a holistic visco-elastohydrodynamical model of *C. elegans* locomotion is difficult. As of this writing, the quantitative physical theory elucidating all the features of our drag force data is lacking; however, we propose two concurrent mechanisms to explain the variations of drag forces with respect to velocity and agar concentration. Horizontal shear gradients around the worm may be responsible for increasing drag on surfaces with thinner liquid layers. Meanwhile, groove formation and increased vertical shear gradients in the lubrication layer under the worm appear to be responsible for increasing drag coefficients at low speeds. Given that over our tested conditions, adhesion force varies by less than one order of magnitude whereas surface stiffness varies over three (28), the surface's mechanical properties are the dominant factor in groove formation during nematode locomotion. Furthermore, it is worth noting that to accurately explain a freely-crawling nematode's kinematics, which have been shown to change appreciably with agar concentration (21), both the viscoelastic forces from the gel and the viscous and capillary forces from the agar's liquid layer must be taken into account.

As a final test of our drag measurements, we used the data obtained from a passive *C. elegans* body to predict the forces generated by an actively moving worm. Using a calibrated cantilever to hold and measure forces from the tail, we quantified the locomotive forces produced by undulatory motions on a wet viscoelastic agar surface. Although the cantilever in our experiment essentially tethers the organism, this only has a minor and localized effect on the worm's interaction with the agar (only slightly lifting it close to the probe tip) and still allows the worm to perform its planar sinusoidal motions.

We show that a simple model based on the dynamics of body shape can use the measured normal and tangential drag coefficients to calculate forces measured from a crawling nematode.

In developing the model, RFT emerges as a sensible fundamental framework because of its simple formulation and its success as a first-order estimator of locomotory forces in many environments. Realizing that RFT alone will not be adequate, we start with its simplest premise, which allows us to quantitatively describe the data with a relatively simple nonlinear mapping made empirically instead of theoretically. These empirical measurements will be useful for system-level models that need estimates of forces due to undulatory movement—for instance, neuronal-based motor control models that are not involved in modeling the fluid and solid-body interactions in detail. If the nonlinearities in drag forces are truly a property of motion on viscoelastic surfaces, this extension of resistive force theory may be applied to other systems, even on the macroscale.

SUPPORTING MATERIAL

Three movies are available at http://www.biophysj.org/biophysj/supplemental/S0006-3495(14)00942-4.

We thank Donald Fu for help with assay development, Adriana Reyna for her skeletonization code, and Stephen Morris, Craig Simmons, and Tim Nayar for helpful discussions.

This work is supported by the Natural Sciences and Engineering Research Council of Canada Discovery Grant, the Canadian Foundation for Innovation, and the Human Frontier Science Program.

REFERENCES

1. Gray, J., and G. J. Hancock. 1955. The propulsion of sea-urchin spermatozoa. *J. Exp. Biol.* 32:802–814.

2. Williams, T. L., S. Grillner, …, S. Rossignol. 1989. Locomotion in lamprey and trout: the relative timing of activation and movement. *J. Exp. Biol.* 143:559–566.
3. Gray, J. 1946. The mechanism of locomotion in snakes. *J. Exp. Biol.* 23:101–120.
4. Maladen, R. D., Y. Ding, …, D. I. Goldman. 2009. Undulatory swimming in sand: subsurface locomotion of the sandfish lizard. *Science.* 325:314–318.
5. Cutter, A. D. 2006. Nucleotide polymorphism and linkage disequilibrium in wild populations of the partial selfer *Caenorhabditis elegans*. *Genetics.* 172:171–184.
6. Barrière, A., and M.-A. Félix. 2005. High local genetic diversity and low outcrossing rate in *Caenorhabditis elegans* natural populations. *Curr. Biol.* 15:1176–1184.
7. Wallace, H. R. 1958. Movement of eelworms: I. The influence of pore size and moisture content of the soil on the migration of larvae of the beet eelworm. *Ann. Appl. Biol.* 46:74–85.
8. Wallace, H. R. 1959. Movement of eelworms: V. Observations on *Aphelenchoides ritzema-bosi* on florists' chrysanthemums. *Ann. Appl. Biol.* 47:350–360.
9. Niebur, E., and P. Erdös. 1991. Theory of the locomotion of nematodes: dynamics of undulatory progression on a surface. *Biophys. J.* 60:1132–1146.
10. Shen, X. N., J. Sznitman, …, P. E. Arratia. 2012. Undulatory locomotion of *Caenorhabditis elegans* on wet surfaces. *Biophys. J.* 102:2772–2781.
11. Sauvage, P., M. Argentina, …, J.-M. Di Meglio. 2011. An elasto-hydrodynamical model of friction for the locomotion of *Caenorhabditis elegans*. *J. Biomech.* 44:1117–1122.
12. Boyle, J. H., S. Berri, and N. Cohen. 2012. Gait modulation in *C. elegans*: an integrated neuromechanical model. *Front. Comput. Neurosci.* 6:10.
13. Sznitman, J., X. Shen, …, P. E. Arratia. 2010. Propulsive force measurements and flow behavior of undulatory swimmers at low Reynolds number. *Phys. Fluids.* 22:121901.
14. Schulman, R. D., M. Backholm, …, K. Dalnoki-Veress. 2014. Dynamic force patterns of an undulatory microswimmer. *Phys. Rev. E Stat. Nonlin. Soft Matter Phys.* 89:050701.
15. Johnson, R. E., and C. J. Brokaw. 1979. Flagellar hydrodynamics. A comparison between resistive-force theory and slender-body theory. *Biophys. J.* 25:113–127.
16. Gray, J., and H. W. Lissmann. 1950. The kinetics of the locomotion of the grass-snake. *J. Exp. Biol.* 26:354–367.
17. Li, C., T. Zhang, and D. I. Goldman. 2013. A terradynamics of legged locomotion on granular media. *Science.* 339:1408–1412.
18. Guo, Z. V., and L. Mahadevan. 2008. Limbless undulatory propulsion on land. *Proc. Natl. Acad. Sci. USA.* 105:3179–3184.
19. Dorgan, K. M., C. J. Law, and G. W. Rouse. 2013. Meandering worms: mechanics of undulatory burrowing in muds. *Proc. Biol. Sci.* 280:20122948.
20. Wallace, H. R. 1969. Wave formation by infective larvae of the plant parasitic nematode *Meloidogyne javanica*. *Nematologica.* 15:65–75.
21. Karbowski, J., C. J. Cronin, …, P. W. Sternberg. 2006. Conservation rules, their breakdown, and optimality in *Caenorhabditis* sinusoidal locomotion. *J. Theor. Biol.* 242:652–669.
22. Berri, S., J. H. Boyle, …, N. Cohen. 2009. Forward locomotion of the nematode *C. elegans* is achieved through modulation of a single gait. *HFSP J.* 3:186–193.
23. Fang-Yen, C., M. Wyart, …, A. D. T. Samuel. 2010. Biomechanical analysis of gait adaptation in the nematode *Caenorhabditis elegans*. *Proc. Natl. Acad. Sci. USA.* 107:20323–20328.
24. Gray, J., and H. W. Lissmann. 1964. The locomotion of nematodes. *J. Exp. Biol.* 41:135–154.
25. Colbert, M.-J., F. Brochard-Wyart, …, K. Dalnoki-Veress. 2010. Squeezing and detachment of living cells. *Biophys. J.* 99:3555–3562.
26. Brenner, S. 1974. The genetics of *Caenorhabditis elegans*. *Genetics.* 77:71–94.
27. Petzold, B. C., S.-J. Park, …, B. L. Pruitt. 2011. *Caenorhabditis elegans* body mechanics are regulated by body wall muscle tone. *Biophys. J.* 100:1977–1985.
28. Nayar, V. T., J. D. Weiland, …, A. M. Hodge. 2012. Elastic and viscoelastic characterization of agar. *J. Mech. Behav. Biomed. Mater.* 7:60–68.
29. Orr, F. M., L. E. Scriven, and A. P. Rivas. 1975. Pendular rings between solids: meniscus properties and capillary force. *J. Fluid Mech.* 67: 723–742.
30. Ding, Y., S. S. Sharpe, …, D. I. Goldman. 2013. Emergence of the advancing neuromechanical phase in a resistive force dominated medium. *Proc. Natl. Acad. Sci. USA.* 110:10123–10128.
31. Sawin, E. R., R. Ranganathan, and H. R. Horvitz. 2000. *C. elegans* locomotory rate is modulated by the environment through a dopaminergic pathway and by experience through a serotonergic pathway. *Neuron.* 26:619–631.
32. Martin, V. M., J. R. Johnson, …, R. D. Burgoyne. 2013. Identification of key structural elements for neuronal calcium sensor-1 function in the regulation of the temperature-dependency of locomotion in *C. elegans*. *Mol. Brain.* 6:39.
33. Omura, D. T., D. A. Clark, …, H. R. Horvitz. 2012. Dopamine signaling is essential for precise rates of locomotion by *C. elegans*. *PLoS ONE.* 7:e38649.
34. Mohammadi, A., J. Byrne Rodgers, …, W. S. Ryu. 2013. Behavioral response of *Caenorhabditis elegans* to localized thermal stimuli. *BMC Neurosci.* 14:66.
35. Johari, S., V. Nock, …, W. Wang. 2013. On-chip analysis of *C. elegans* muscular forces and locomotion patterns in microstructured environments. *Lab Chip.* 13:1699–1707.
36. Backholm, M., W. S. Ryu, and K. Dalnoki-Veress. 2013. Viscoelastic properties of the nematode *Caenorhabditis elegans*, a self-similar, shear-thinning worm. *Proc. Natl. Acad. Sci. USA.* 110:4528–4533.
37. Colbert, M.-J., A. N. Raegen, …, K. Dalnoki-Veress. 2009. Adhesion and membrane tension of single vesicles and living cells using a micropipette-based technique. *Eur. Phys. J. E Soft Matter.* 30:117–121.
38. Gonzalez-Rodriguez, D., L. Bonnemay, …, F. Brochard-Wyart. 2013. Detachment and fracture of cellular aggregates. *Soft Matter.* 9:2282.
39. Mitrossilis, D., J. Fouchard, …, A. Asnacios. 2010. Real-time single-cell response to stiffness. *Proc. Natl. Acad. Sci. USA.* 107:16518–16523.